High-Throughput Pressure Dependent DFT Investigation of Herringbone Polycyclic Aromatic Hydrocarbons (HB-PAHs): Part 1. Pressure Dependent Structure Trends

Mahmoud Hammouri^a, Taylor M. Garcia^b, Cameron Cook^a, Stephen Monaco^b, Sebastian Jezowski^c, Noa Marom^d, and Bohdan Schatschneider^{a,b*}

Abstract: External pressure is known to alter the molecular and structural conformations of soft materials, leading to changes in the intermolecular interactions as well as the inherent physical properties. In part 1 of a two-part investigation, we introduce pressure within the dispersioninclusive density functional theory framework (DFT+vdW) to perturb the structures and intermolecular interactions of 42 crystalline, herringbone polycyclic aromatic hydrocarbons (HB-PAHs). The applied pressure results in alterations of the crystalline unit cells, intermolecular interactions, and molecular conformations. In general, the unit cell lengths/volumes decrease monotonously with increasing pressure. Hirshfeld surface analysis typically reveals an increase in the C···H and C···C intermolecular close contact fractions with increased pressure, and a decrease in the H···H interactions. The increase in the C···H and C···C intermolecular interactions enhances the C-H··· π and π ··· π interactions, decreasing intermolecular repulsion and increasing electron exchange interactions through increased molecular orbital overlap. Discontinuous pressure dependent changes in the unit cell parameters and intermolecular close contact fractions of several structures are observed, indicating the possibility of some phase transitions. In part 2 of this two-part investigation, the structural changes observed here are linked to changes in the electronic properties of these systems.

1. Introduction:

Polycyclic aromatic hydrocarbons (PAHs) are a family of organic molecules comprised of two or more aromatic rings. In the solid state, these materials exhibit five typical crystalline packing motifs, 1) herringbone (HB) 2) sandwich herringbone (SHB) 3) beta herringbone (β -HB) 4) beta (β) and 5) gamma (γ). Each motif is classified *via* the π -degree parameter (π^o), which is derived from the percent C···C intermolecular interactions present on the Hirshfeld surface (%C···C) and the intermolecular interplanar angle (θ) existing between neighboring molecules. This study is focused on herringbone PAHs (HB-PAHs), characterized by little cofacial intermolecular interactions (*i.e.*, %C···C \approx 0 on the Hirshfeld surface) and significant edge-to-face (C···H) and edge-to-edge (H···H) intermolecular interactions .^{1,6} The Hirshfeld intermolecular close contact fractions, as well as the intermolecular distances and spatial orientations, will ultimately help us elucidate the changes occurring in the crystalline and electronic structures.⁷

^a Department of Chemistry and Biochemistry, California State Polytechnic University, Pomona, 3801 W Temple Ave, Pomona, CA 91768 United States

^b The Pennsylvania State University, Fayette-The Eberly Campus, 2201 University Drive, Lemont Furnace, Pennsylvania 15456, United States

^c Department of Chemistry, Murry State University, 102 Curris Center, Murry, KY 42071

^d Department of Materials Science and Engineering, Department of Chemistry, and Department of Physics, Carnegie Mellon University, 5000 Forbes Avenue, Pittsburgh, PA 15213-3890

The unique optoelectronic properties of PAHs have led to extensive experimental and theoretical studies over the last four decades. The use of such materials in electronic applications requires a deep understanding of the relationship between the molecular/crystalline structures chemical/physical properties. One way of tuning the distances/orientations in crystalline PAHs, and the resulting electronic properties, is by applying high pressure. In PAHs, application of high pressure has delivered a wide range of new polymorphs with novel electronic properties, including organic superconductors.⁸ HB-PAHs are observed to undergo phase transitions in the low pressure⁹⁻¹¹ and high pressure¹¹ regimes. The primary effect of applying pressure on crystalline HB-PAHs is flattening of any twists in the molecular structures and an increase in C···C and C···H intermolecular close contacts in the crystal, accompanied by a decrease in the H···H interactions. 5,12,13,14 In oligoacenes, the response of naphthalene, anthracene, tetracene, and pentacene to pressure has been shown to depend on their crystal symmetries. 13 In the same study, it was found that the four oligoacenes become more cofacially orientated within the unit cell with increased pressure.

The relatively weak nature of the van der Waals (vdW) forces binding HB-PAHs allows for easy perturbation of the crystalline structure with low-to-moderate pressures (> 0.1 GPa), and in some cases enables the formation of new polymorphs and physical properties. 15-17 It has been shown both theoretically and experimentally that pressure alters the molecular conformation in HB-PAHs such as poly(para-phenylenes), 18 picene, 16 oligoacenes, 19,20 triphenylene, 21 and rubrene.²² External pressure can change other properties of the molecular components (e.g., aromatic character) that are ultimately linked to the electronic properties of the crystals. Such changes have been shown to increase the internal energy and enthalpy of the systems.²³ A clear example of pressure induced optoelectronic changes has been demonstrated by the reversible color change that occurs in the crystals of benz[a]anthracene with increased pressure.²⁴ To study the effect of structural changes on the optical and transport properties, Heimel et. al. investigated the pressure dependence of the lattice parameters a and b of five poly-(para-phenylenes). 12 In addition to the cofacial alignment, the authors found poly-(para-phenylenes) to be less compressible as the number of the phenyl rings increases. Their results indicate a decrease in the band gap and an increase in the electronic conductivity, which can be explained by the increase in the orbital overlap between adjacent molecules. 8,12,25,26

In order to gain a detailed understanding regarding the effect crystal structure has on the physical properties of PAHs, we applied high pressure (up to 20 GPa) to 42 HB-PAHs and monitored the effect of the resulting changes in the intermolecular interactions on the electronic structure. In Part 1 of this two-part investigation into the pressure dependent properties of PAHs, we report the structural changes as a function of pressure. The structural changes are investigated by using dispersion inclusive density functional theory (DFT+vdW) to perform structural relaxations under pressure and by Hirshfeld surface analysis of the intermolecular contacts in the resulting structures. In Part 2 [ref], we provide a detailed analysis of how the electronic behavior of these materials changes with increased pressure.

2. Computational Method

Our previous high pressure work on polyacenes, ¹⁹ rubrene, ²² indole, ¹⁵ and TCNE²⁷ shows that the Perdew-Burke-Ernzerhof generalized gradient approximation ²⁸ with the Tkatchenko-Scheffler pairwise dispersion correction ²⁹ (PBE+vdW), as implemented in the CASTEP code, can accurately model the pressure dependent structural response of organic molecular crystals (OMCs) that exhibit a variety of intermolecular forces. ⁵ In the case of the oligoacenes

(naphthalene through pentacene), we were able to reliably model the systems with structural agreement within ~3% up to 20 GPa. PBE+vdW was also able to capture the phase transition behavior of both tetracene and pentacene despite the 0 K constraint of DFT, as well as the symmetry constraints imposed by the CASTEP software. For triclinic rubrene, PBE+vdW was able to accurately predict the pressure dependent behavior of the unit cell parameters and density until the solid-solid phase transition. PBE+vdW was also able to replicate the phase transition, albeit at a higher hydrostatic pressure, owing to the solid-solid phase transition activation barrier and lack of thermal energy. For indole, PBE+vdW was able to replicate the structural descriptors at ambient pressures as well as realistically model the pressure induced solid-solid phase transition. The use of DFT+vdW in our previous work of polyacene, produced variations in the unit cell parameters $\leq 2\%$ compared to experiment at ambient pressure.³⁰ The pressure dependent structural changes for naphthalene, anthracene, tetracene, and pentacene agree with experiment. 5,27,31 At ambient pressure, the variations of lattice parameters a, b, and c of triclinic rubrene are 0.6%, 1.7%, and 0.9%, respectively compared to experiment.³² The pressure dependent structural changes of triclinic rubrene agree very well with experiment ¹⁴ for pressure less than 6 GPa, at which point a phase transition takes place. A similar phase transition was captured using DFT+vdW, but at ~16 GPa. Considering how well PBE+vdW has replicated the ambient as well as the temperature and pressure dependent structural changes of a wide variety of OMCs, we are reasonably confident that the predicted high pressure structures presented here offer realistic insight into each system's pressure dependence. It should be noted that the most thermodynamically stable phase may not necessarily be derived by simply applying pressure at 0 K. Ideally, a global optimization search would be preferable for all structures at all pressures [Ref Ashcroft]. However, this approach is prohibitively expensive, computationally, considering the large number of structures being investigated.

From the standpoint of a high-throughput investigation, in which ~1700 geometry optimizations were performed on fairly large periodic systems, a balance between chemical accuracy, reproducibility, comparability, and speed needed to be met. One way to ensure these criteria are met is to select a standard set of input parameters for all calculations which has provided reliable outputs in previous investigations. With this in mind, all periodic calculations were conducted as done in our previous PAH investigations ^{6,19} using PBE+vdW as implemented in the Cambridge Serial Total Energy Package (CASTEP) electronic structure code. ³³ The electronic wave functions are expanded using a plane-wave basis set in CASTEP, and the energy cutoff was set at 750 eV for all structures. Other convergence criteria are set as follow: total energy, max force, max stress, max displacement, and SCF iterations are 5 x 10⁻⁶ eV/atom, 0.01 eV/Å, 0.02 GPa, 5 x 10⁻⁴ Å⁻¹ and 5 x 10⁻⁷ eV/atom, respectively. For the k points sampling, we chose the Monkhorst-Pack³⁴ scheme such that the k point separation is about 0.07 Å⁻¹. Norm-conserving pseudopotentials (NCPP) were employed for C and H atoms.

The geometry (lattice parameters and atomic coordinates) of the crystal structures was optimized at 0.5 GPa increments, using the Broyden–Fletcher–Goldfarb–Shanno (BFGS) minimizer which uses a starting Hessian that is recursively updated during optimization. ³⁵ By default, CASTEP imposes symmetry on crystalline structures during geometry optimizations, never allowing a system to *decrease* its symmetry in order to speed up the calculations. As this is a high-throughput investigation, this is a desirable option. The starting structures were obtained from the data sets available in the Cambridge Structural Database (CSD). ³⁶ The crystals studied here are denoted by their Cambridge Crystallographic Database (CSD) reference codes and are listed in **ESI Table S1**. All geometry optimized structures and properties have been uploaded to

the Organic Crystal Structure and Electronic Properties Database (OCSEPD) at organic crystalbandgaps.org. We note that the structure of 1,2,3,4,6,8,9,10,11,13-decaphenylpentacene (VEBJAO) had issues with energy convergence at pressures higher than 1.5 GPa. Despite trying a myriad of solutions, convergence could not be achieved at high pressures.

Hirshfeld surfaces and the corresponding fingerprint plots were generated using Crystal Explorer 3.1.³⁷ For the intermolecular interactions within the crystal structures, we constructed fingerprint plots *via* the deconvolution of the Hirshfeld surface. Hirshfeld surface analysis has been used previously as a powerful tool for determining intermolecular interactions within molecular crystals.^{1,15,19} (see Refs^{23,38-40} for detailed discussion of Hirshfeld surfaces and their applications).

3. Results and Discussion

General analysis of structural evolution with pressure. We begin by discussing 3.1.1. the general pressure dependent structural response of the HB-PAHs and proceed to discuss the characteristic responses of several well-known HB-PAH families. The structural analysis of 42 HB-PAHs under hydrostatic pressure is based on methods previously used by us to investigate the property-structure relationships of crystalline PAHs and other small OMCs under both ambient and high pressure conditions. 1,6,10,15,19,22 Here, as well as in the previous investigations, PBE+vdW provides excellent agreement between the calculated and experimental structural descriptors (e.g., lattice parameters, internal molecular geometries, intermolecular close contacts, and density). The agreement between the calculated and experimental unit cell parameters and densities are within $\sim 2\%$ for structures at nearly all pressures. Comparisons with new experimental parameters for several structures is shown in Figs S1-S3 in the electronic supplemental information (ESI). Agreement within 2% of experiment was also found for the ambient pressure intramolecular geometries (specifically C-C distances). Similarly, agreement of the intermolecular geometries was achieved between the PBE+vdW and experimental structures as monitored via Hirshfeld surface close contact fractions. It is observed in the pressure dependent plots of the structural descriptors (unit cell parameters, density, etc.) that most HB-PAHs have similar pressure dependent structural responses. Some systems, however, exhibit anomalous pressure responses. These cases are described in detail below with comparisons to experiments, where available.

Naphthalene (NAPHTA04) will be used as a representative example to illustrate the general pressure dependent structural trends of the HB-PAHs, as its pressure dependent behavior is typical of most HB-PAHs studied here. The crystal structure of naphthalene and the pressure dependent response of the crystal parameters is shown in **Fig. 1**. It is observed that the lattice parameters, a, b, and c, decrease upon pressurization by 18%, 10.8%, and 9.6%, respectively. The volume is shown to decrease by 36.3%. Both results agree well with experiment.⁵ The pressure dependent volume change associated with naphthalene compares well with the average volume decrease of all HB-structures studied here (34.2%) as shown in the percent volume change histogram of **Fig 2**. It is interesting to note that lattice parameter a decreases about 1.7 times as much as the other parameters due to its association with the π -stacking direction of the crystal. It is a general trend that HB-PAH structures collapse about twice as much along the π -stacking direction than any other direction, due to the decrease in the intermolecular interplanar angle, θ . ^{12,13,41} The exponential decay of the lattice parameters, as seen for NAPHTA04, is also found for nearly all HB-PAHs, as shown in **ESI Figs S5-S7**.

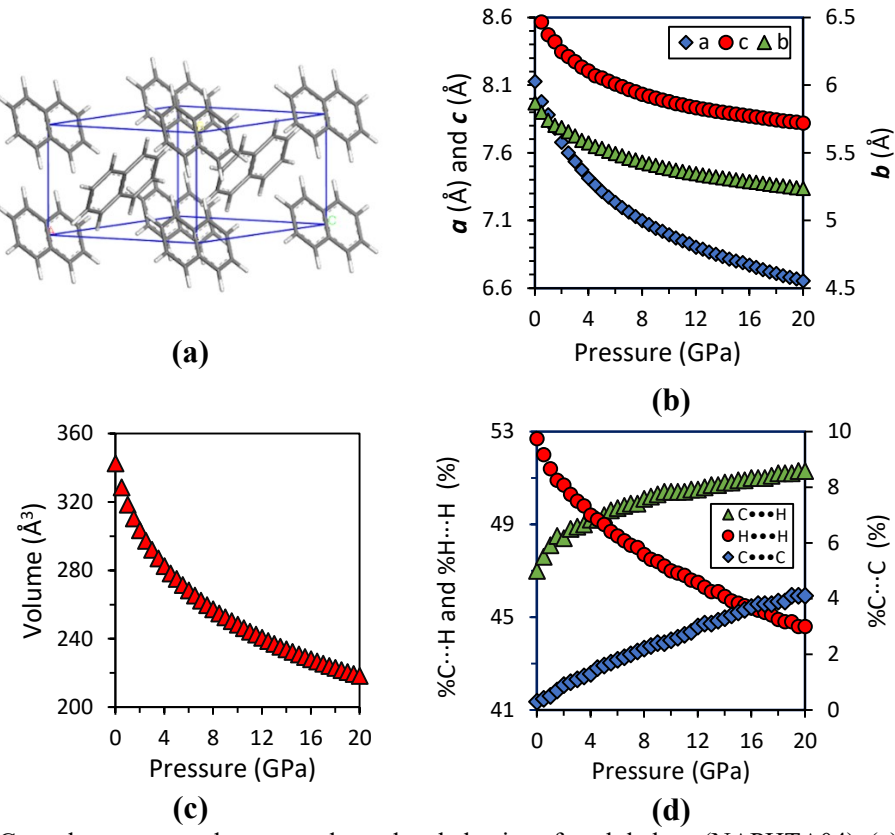


Figure 1. Crystal structure and pressure dependent behavior of naphthalene (NAPHTA04). (a) NAPHTA04 structure at 0 GPa. (B) Unit cell parameters (c) volume and (d) Hirshfeld surface intermolecular close contact fractions as a function of pressure for naphthalene. Secondary and principle axes are on the same scale.

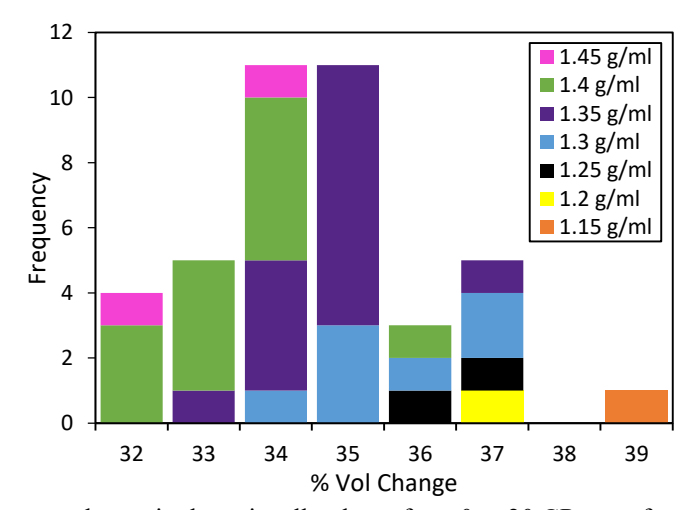


Figure 2. Percent change in the unit cell volume from 0 to 20 GPa as a function of density at 0 GPa for all HB-PAHs that had a full set of pressure dependent data. The densest structures at 0 GPa show the smallest percent change in the unit cell volume.

In order to investigate the pressure dependence of the internal crystalline geometry, the fractions of C···C, C···H, and H···H intermolecular contacts (%C···C, %C···H, and %H···H) as derived from Hirshfeld surface analysis are plotted for naphthalene as a function of pressure in

Fig 1. The %C···C has the smallest contribution to intermolecular interactions at 0 GPa, while the C···H, and H···H interactions make up the majority of intermolecular close contacts. This trend is observed for all HB-PAHs as seen in the intermolecular close contact fraction histograms of **Fig 3**, where the average %C···C, %C···H, and %H···H are 2.7%, 48.5%, and 48.7%, respectively.

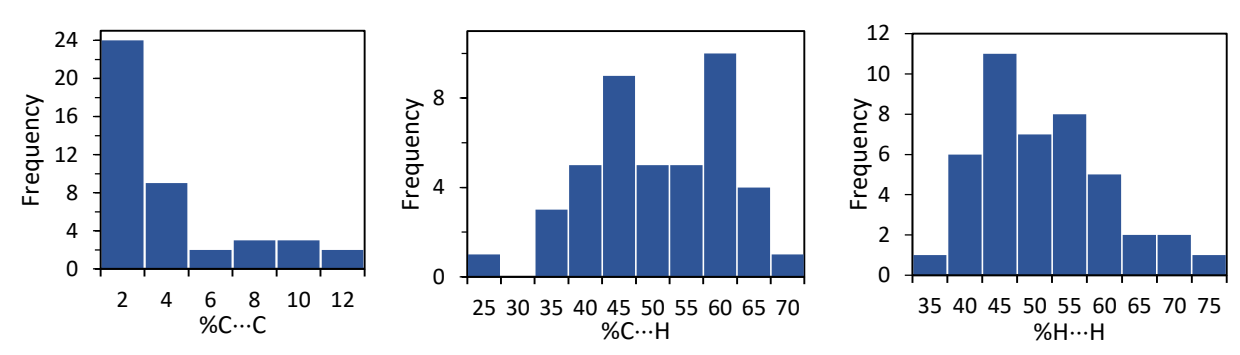
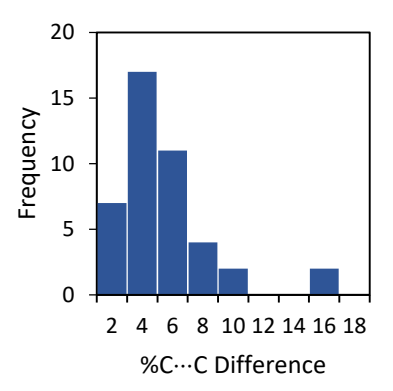
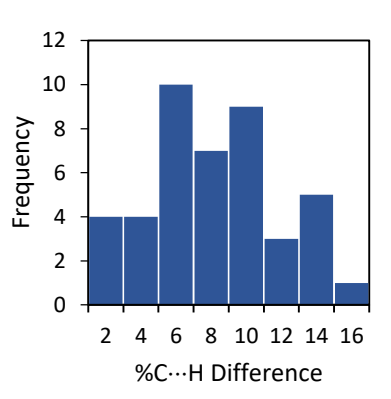


Figure 3. Distribution of Hirshfeld surface intermolecular close contact fractions at 0 GPa for all HB-PAHs.

As seen in **Fig 1**, the C···C and C···H interactions increase with increasing pressure, whereas the H···H interactions decrease. Most HB-PAH structures have similar close contact fraction trends, as evident in the absolute close contact fraction change histograms, shown in **Fig 4** (also see **ESI Figs S8-S10**). For naphthalene, there is a ~4% increase in %C···C from 0 to 20 GPa, a ~4% increase in %C···H, and an ~8% decrease in %H···H. The average change in %C···C, %C···H, and %H···H from 0 to 20 GPa for all HB-PAHs here is +4.4%, +7.0%, and -10.1%, respectively. These changes in the intermolecular interactions are not only a function of decreasing unit cell parameters but are also a function of an increase in the interplanar angle $(\theta)^{27,31}$ upon pressurization. The increase in θ helps alleviate repulsive interactions within the structure and effectively increases the packing efficiency. The increase in θ and the C···C and C···H contacts occurs because increasing the cofacial orientation of the molecules within the unit cell reduces the electrostatic repulsions resulting from edge-to-edge interactions. This also allows for the largest changes in the unit cell parameters to occur along the stacking direction. 13,41

Different theoretical and experimental studies on PAHs have revealed varying structural and optical responses to external pressure, 5,23,37-43 where pressure induced solid-solid phase transitions are commonly observed. Despite previous success capturing pressure induced phase transitions in PAHs using DFT, 17,19,21 the accuracy is somewhat limited by the fact that geometry optimization under pressure is performed in the ground state at 0 K. So, although DFT correctly detects phase transitions in some cases, it fails in others because the thermal energy needed to overcome transition barriers is missing. In this study, no pressure induced space group transitions were observed. However, as highlighted below, discontinuities in the pressure dependent structural descriptor plots of several systems indicate that some significant molecular/crystalline rearrangements have occurred. We have provided the structural data of all the PAHs studied here (at every pressure) in the Organic Crystal Structure and Electronic Properties Database (OCSEPD) at organiccrystalbandgap.org.





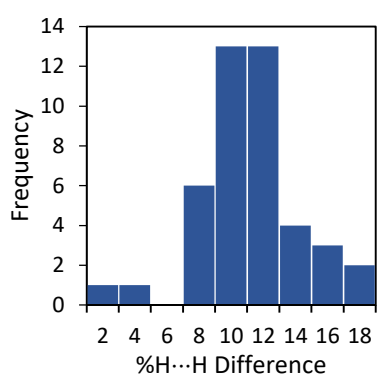


Figure 4. Absolute difference between the Hirshfeld surface close contact fractions at 0 GPa and 20 GPa for all HB-PAHs. For the %C···C and %C···H, the changes are in the positive direction while for the %H···H the change is always negative.

3.1.2 Aryl Oligoacenes Derivatives (Cruciforms): There are three aryl substituted oligoacenes in the HB motif that show varying pressure dependent behavior: 9,10diphenylanthracene (DPANTR01), rubrene (QQQCIG04), and 5,7,12,14-tetraphenylpentacene (VEBJES) (structures shown in Fig. 5). These structures are of interest to device manufacturers because they have shown high charge carrier mobilities as well as possible singlet fission (SF) activity.^{23,45-48} The structure of DPANTR01 contains an anthracene backbone with two phenyl groups substituent at the 9 and 10 positions tilted by ~66° with the anthracene backbone. The unit cell of DPANTR01 is from the most stable α -polymorph, which is monoclinic with C2/cspace group. ^{49,50} Rubrene has a tetracene backbone and four phenyls substituent at the 5, 6, 11, and 12 positions. The most common polymorph of rubrene is orthorhombic which has a CMCA space group where the phenyl groups are twisted by $\sim 77^{\circ}$ with the tetracene moiety.⁵¹ It is interesting to note that the orthorhombic polymorph investigated here contains about 2.5 times the amount of π -stacking interactions at ambient conditions (6.4% at 0 GPa) compared to other HB-PAHs (the average is 2.7% at 0 GPa). The third aryl substituted acene is 5,7,12,14tetraphenylpentacene (VEBJES), which is monoclinic with a C2/c space group and Z=4.⁵² The VEBJES structure has a pentacene backbone with four lateral phenyl groups substituent at 5,7,12, and 14 positions which have varying twists to the pentacene backbone (see Figs 5 & 10).

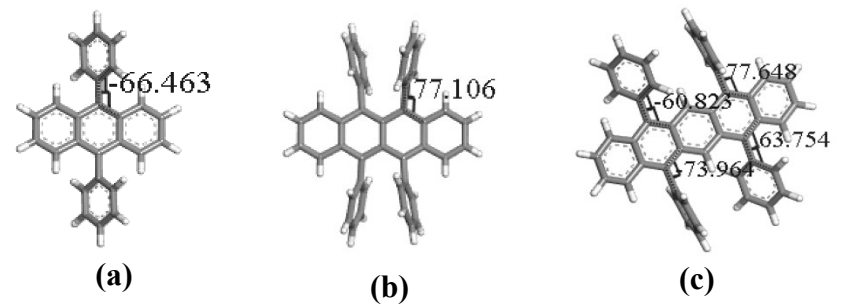


Figure 5. Molecular structure of (a) DPANTR01, (b) QQQCIG04, and (c) VEBJES.

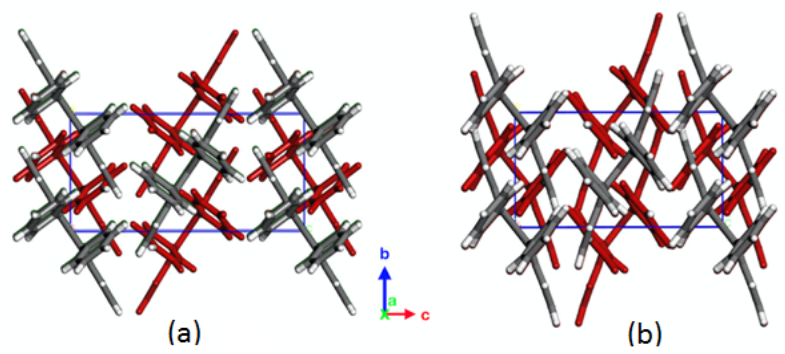


Figure 6. Crystal structure of rubrene (QQQCIG04) at (a) ambient and (b) 20 GPa pressure. Grey and white molecules are in the foreground and red molecules are in the background.

On the molecular level, the tetracene backbone of QQQCIG04 is flat within the crystal at 0 GPa, but as pressure increases the tetracene backbone kinks to accommodate the tighter packing (see **Fig 6**). This pressure dependent change was observed experimentally for triclinic rubrene, ²² yet no change in the space group was found up to 7.1 GPa. ¹⁴ Excellent agreement of the calculated and experimentally determined lattice parameters for the triclinic phase are shown in the **SI** of our previous work. ²³ The lattice parameter response of QQQCIG04 to pressure is plotted in **Fig 7** as well as those for DPANTR01 and VEBJES. As seen for rubrene, lattice parameter c (along the π -stacking direction) is compressed the most (~20%) whereas a and b only compress approximately half as much (7% and 11%, respectively).

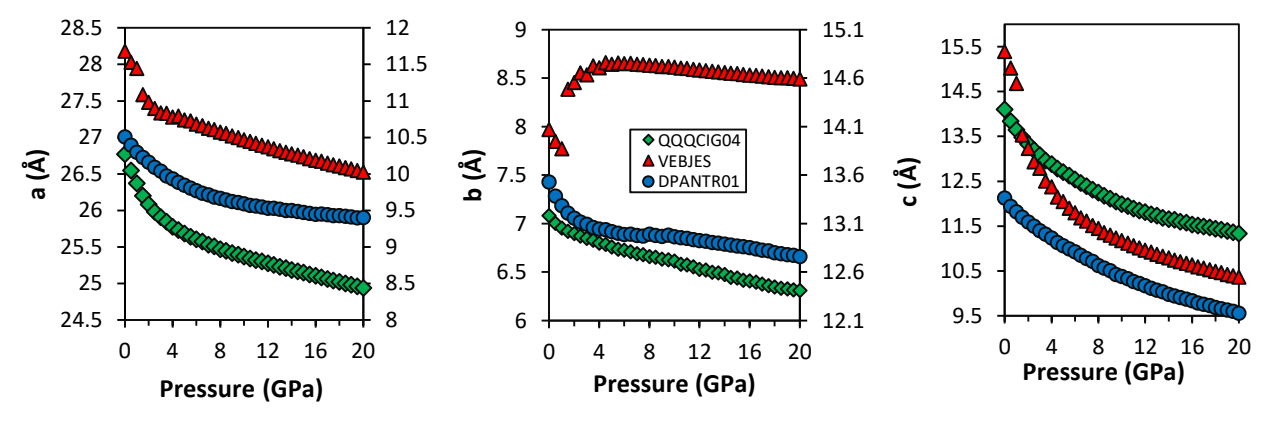


Figure 7. Lattice parameters a, b, and c as a function of pressure for QQQCIG04, VEBJES, and DPANTR01. Parameters a and b of DPANTR01 are plotted on the secondary axis (same scale as primary axis).

The response of the lattice parameters a, b, and c to pressure for DPANTR01 are comparable to that of QQQCIG04, decreasing continuously by 11%, 6%, and 21% respectively. The shorter anthracene backbone of DPANTR01 remains planar up to 20 GPa. However, the phenyl group torsion angle changes from 66° at ambient pressure to 42° with the anthracene backbone, see Fig. 8. The a and c parameters of VEBJES undergo discontinuous decreases between 1.0 GPa and 1.5 GPa while the b parameter discontinuously increases, hinting at a phase transition. Inspection of the structures before and after the discontinuous changes show that the phase transition can be characterized by a slipping of the molecular layers leading to an increase in β . This shrinks a and c. The molecules also rotate, decreasing the intermolecular interplanar angle (increasing coplanarity) This allows for tighter packing along the π -stacking direction and enlarges b. No

change in the space group was observed. Representative figures of the phase transition are provided in SI Fig S11.

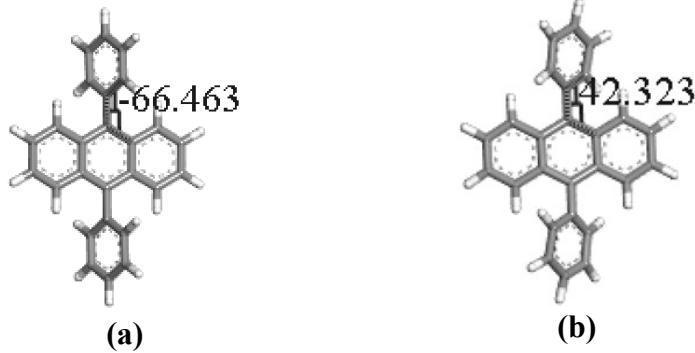


Figure 8 Molecular structure of DPANTR01 at 0 GPa and 20 GPa. (a) 0 GPa and (b) 20 GPa

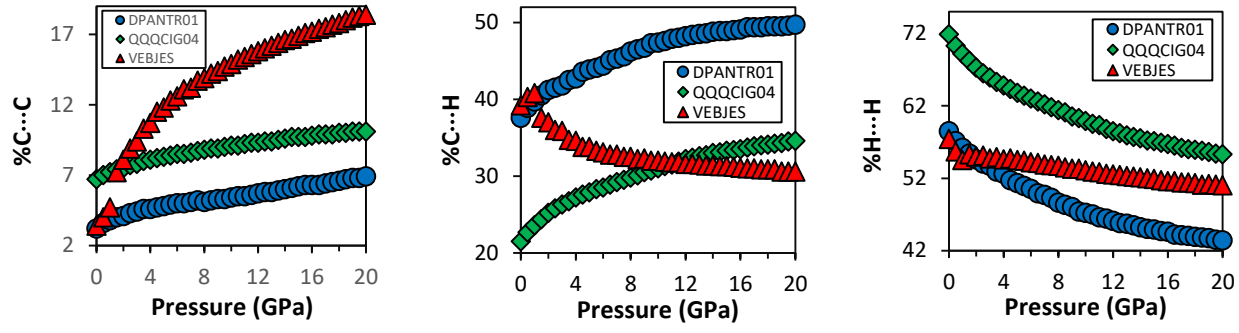


Figure 9. Relative intermolecular close contact fractions as a function of pressure for DPANTR01, QQQCIG04, and VEBJES.

The changes in the unit cell parameters are accompanied by changes in the intermolecular close contact fractions as shown in **Fig 9**. The pressure dependence of %C···C, %C···H, and %H···H is very similar for DPANTR01 and QQQCIG04, where the %C···C increases by ~4% and ~3% respectively, while the %C···H increases by ~12% and ~13%, and the %H···H decreases by 14% and ~17%. These intermolecular close contact changes are linked directly to the changes in the lattice parameters, though the specifics vary for each structure: For DBANTR01, when a, b and c decrease, the phenyl rings interact more with the anthracene backbone by decreasing the torsion angle and bending the anthracene-phenyl bond, increasing the %C···C and %C···H while decreasing the %H···H (see **Fig 8**). For QQQCIG04, when b decreases the phenyl groups from neighboring molecules pack closer together, increasing %C···H, and when c decreases the tetracene backbones approach each other in the π -stacking direction (see **Fig 6**). When a decreases, the phenyl groups of neighboring molecules slide between each other, decreasing the H···H interactions.

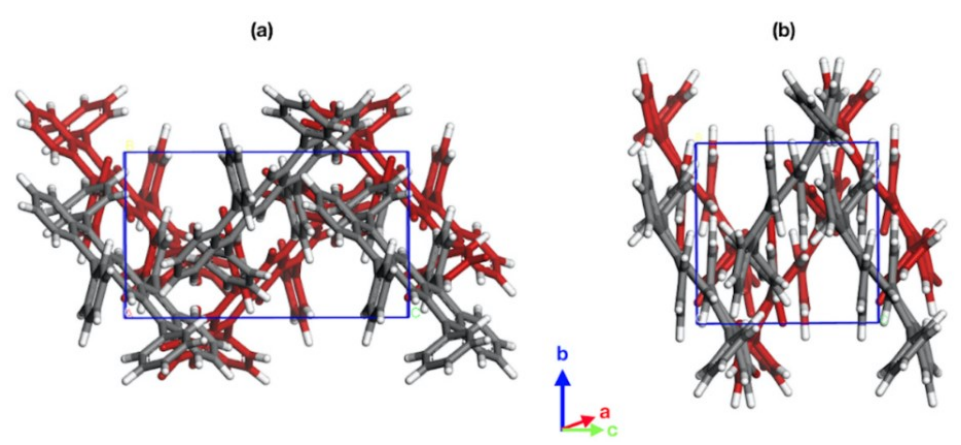


Figure 10 Crystal structure of VEBJES at (a) ambient and (b) 20 GPa pressure. Red Molecules are in the back layer.

A very different pressure dependence in the intermolecular close contact fractions is observed in the case of VEBJES. Here, there are discontinuous changes in all contacts between 1.0 to 1.5 GPa associated with the phase transition. Over the 0 to 20 GPa range, the %C···C increases by ~15%, whereas the %C···H and %H···H interactions decrease by ~9% and ~6%, respectively. From **Fig 10**, one observes that the VEBJES molecules become kinked, and more parallel to lattice vector \boldsymbol{b} , with increased pressure. Also, lattice parameter \boldsymbol{c} shrinks ~12% more than in the case of DBANTR01 and QQQGIG04 do to the slips in the molecular layers. This series of events makes the molecules stack more cofacially as compared to DBANTR01 and QQQGIG04, increasing the C···C interactions while decreasing both the C···H and H···H interactions.

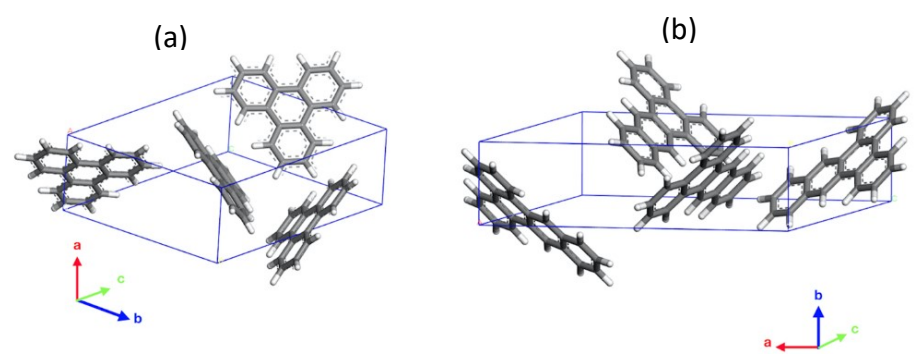


Figure 11. Crystal structure of (a) TRIPHE12 and (b) SANQII at ambient pressure.

3.1.3 Triphenylenes: In this section, two similar structures, triphenylene (TRIPHE12) and benzo[b]triphenylene (SANQII) are discussed (structures shown in **Fig 11**). TRIPHE12 crystals are orthorhombic with a P2₁2₁2₁ space group and Z=4⁵⁰ while SANQII crystals are monoclinic with a P2₁ space group and Z=4⁵³. Triphenylene-based polymers have shown potential for applications in light emitting diodes (LEDs),⁵⁴ while benzo[b]triphenylenes are potential candidates for other optoelectronic devices^{55,56} and discotic liquid crystals.⁵⁷ TRIPHE12 is fairly robust and found to be more stable under high pressure as compared to phenanthrene. This may be attributed to the additional Clar-sextets and fully benzenoid character in TRIPHE12.²¹

The pressure dependence of a, b, and c of TRIPHE12 and SANQII is shown in Fig 12. For TRIPHE12, a, b, and c continuously decreases upon pressurization up to 20 GPa by 13%, 14%, and 11%, respectively. These results agree nicely with a combined experimental and theoretical investigation²¹ on the crystalline triphenylene as shown in ESI Fig S1. In both investigations, no polymorphic phase transitions of TRIPHE12 were observed. In the case of benzo[b]triphenylene (SANQII), from 0-7.5 GPa, a, b, and c decrease continuously with respect to increasing pressure. Then from 7.5-8.0 GPa, a, b, and c decreases by 16% whereas a and c increase by 9.8% and 8.4%, respectively. Then above 8 GPa, a, b, and c decrease continuously. There is no change in the space group associated with this large structural rearrangement. The phase transition can be characterized by a decrease in the intermolecular interplanar angle, making the molecules significantly more coplanar. This elongates a and c while allowing for tighter packing along the π -stacking direction (shrinking a). Representative figures of the phase transition can be found in SI Fig S12.

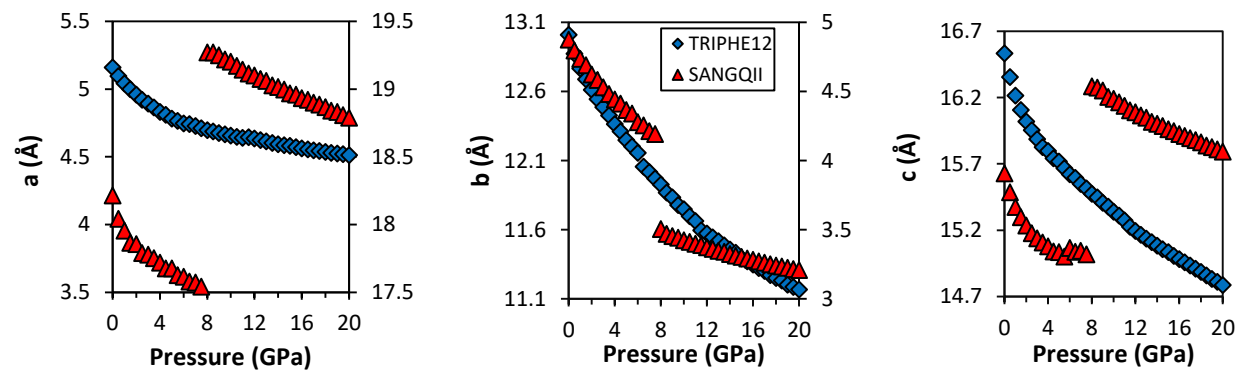


Figure 12. Lattice parameters **a**, **b**, and **c** as a function of pressure for TRIPHE12 (primary axes) and SANQII (secondary axes). Secondary and primary axis are on the same scale.

The intermolecular close contact fractions as a function of pressure for TRIPHE12 and SANQII are plotted in Fig 13. TRIPHE12 exhibits the typical trend of the C···C and C···H interactions increasing with pressure (3.0% and 7.4%, respectively) while the H···H interactions decrease by ~10%. In contrast, SANQII exhibits unique behavior. The C···C interactions increase continuously by 5.1% with pressure up to 7.5 GPa, at which point a discontinuous increase of about 7% associated with the phase transition is observed, followed by a continuous increase of about 2% until 20 GPa. For the C···H interactions, there is an atypical decrease of about 3% upon increased pressure to 7 GPa, then a discontinuous decrease of about 13% associated with the phase transition is observed at 7.5 GPa followed by an ~1% increase until 20 GPa. The H···H interactions decrease (as expected) by ~3% until 7 GPa, followed by an atypical 6% increase at 7.5 GPa, and then a ~2% decrease until 20 GPa. This unusual behavior of SANQII occurs because as the pressure approaches 7.5 GPa, the molecules within the unit cell are steadily approaching each other in a way that increases cofacial interactions while decreasing the edgeto-face and edge-to-edge interactions. Then at 8 GPa the molecules abruptly become more parallel to a-c plane, which makes their interactions significantly more cofacial. This manifests in a discontinuous increase in a and c whereas b decreases as shown in Fig. 12.

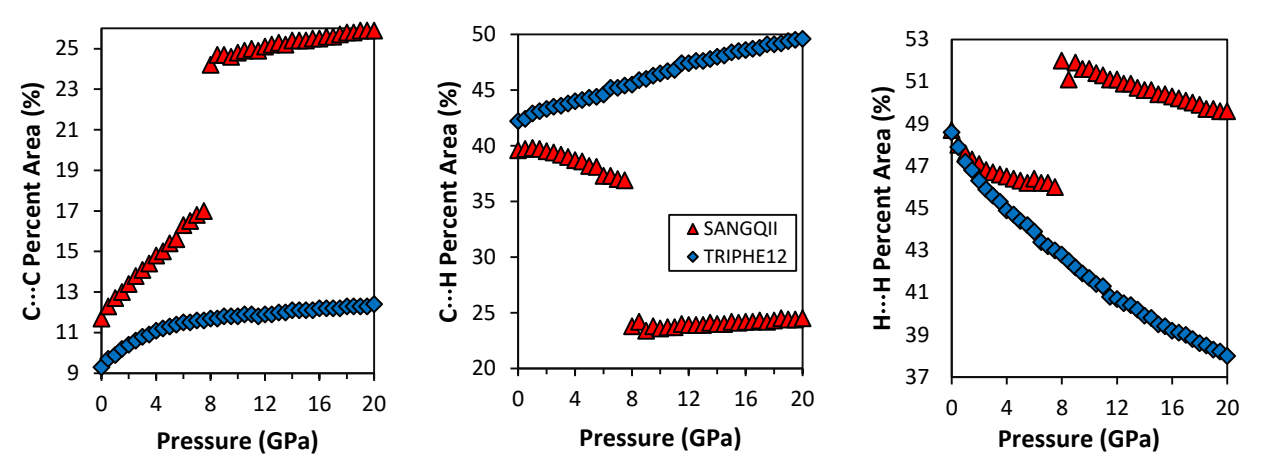


Figure 13. Relative intermolecular close contact fractions as a function of pressure for TRIPHE12 and SANOII.

3.1.4 Poly (*para*-phenylenes): In this section, we turn our focus to poly (*para*-phenylenes), which include: benzene (1P, BENZEN), biphenyl (P2P, BIPHEN), *p*-terphenyl (P3P, TERPHE02), *p*-quaterphenyl (P4P, QUPHEN), *p*-quinquephenyl (P5P, ZZZNKU01), *p*-sexiphenyl (P6P, ZZZNTQ01), and *p*-septiphenyl (P7P, LIMCUF). Poly(*para*-phenylene) structures are comprised of phenyl rings connected by single C-C bonds in the *para* positions. At ambient conditions, 2P⁵⁸, P3P⁵⁹, and P4P⁶⁰ crystallize in a P2₁/a monoclinic structure, whereas P5P⁶¹, P6P⁶¹, and P7P⁶¹ crystallize in a P2₁/c monoclinic structure. Benzene⁶² is characterized by an orthorhombic P*bca* space group, which results in unique properties, compared to the rest of the group.

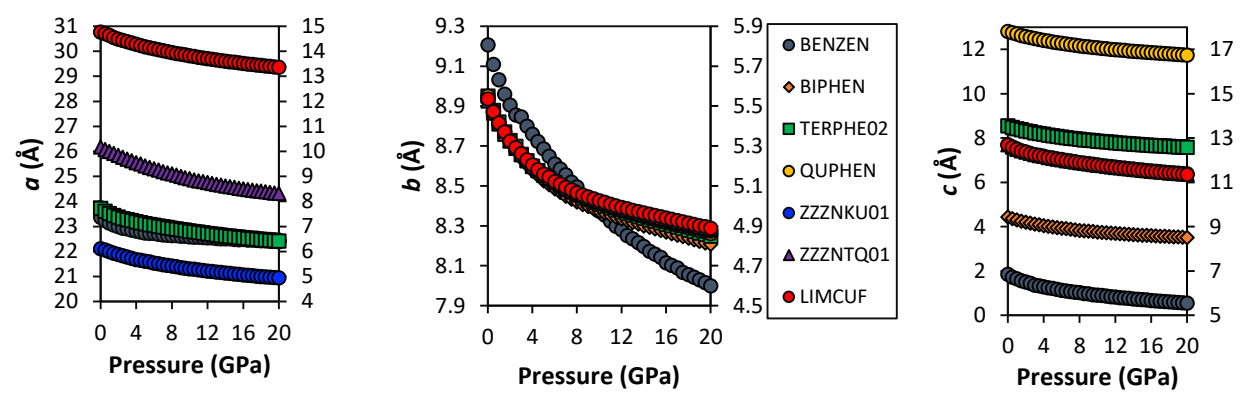


Figure 14. Lattice parameters **a**, **b**, and **c** as a function of pressure for poly(*para*-phenylenes). For **a**, BENZEN, BIPHEN, TERPHE02, and QUPHEN are on secondary axis (long molecular axis for structures on primary axis and 2nd short molecular axis for molecules on secondary axis) - BENZEN, BIPHEN, and QUPHEN are hidden under TERPHE02. For **b**, BENZEN on primary axis (1st short molecular axis for all structures). For **c**, BENZEN, BIPHEN, TERPHE02, and QUPHEN are plotted on secondary axis (2nd short molecular axis for structures on primary axis and long molecular axis for molecules on secondary axis) – ZZZNTQ01 and ZZZNKU01 are hidden under LIMCUF. Secondary and primary axis are on the same scale.

The pressure dependent response of the lattice parameters for the poly(para-phenylenes) is shown in Fig. 14. Comparisons between experimental and calculated unit cell volumes are provided in ESI Fig S2 and are within 3% for all pressures. The percentage decrease in a, b, and c for two pressure ranges 0-6 GPa and 0-20 GPa is shown in ESI Table S1. Within the range of

0-6 GPa, our calculations show that the lattice parameter a (c) decreases more than b agreeing well with previous experimental work.³¹

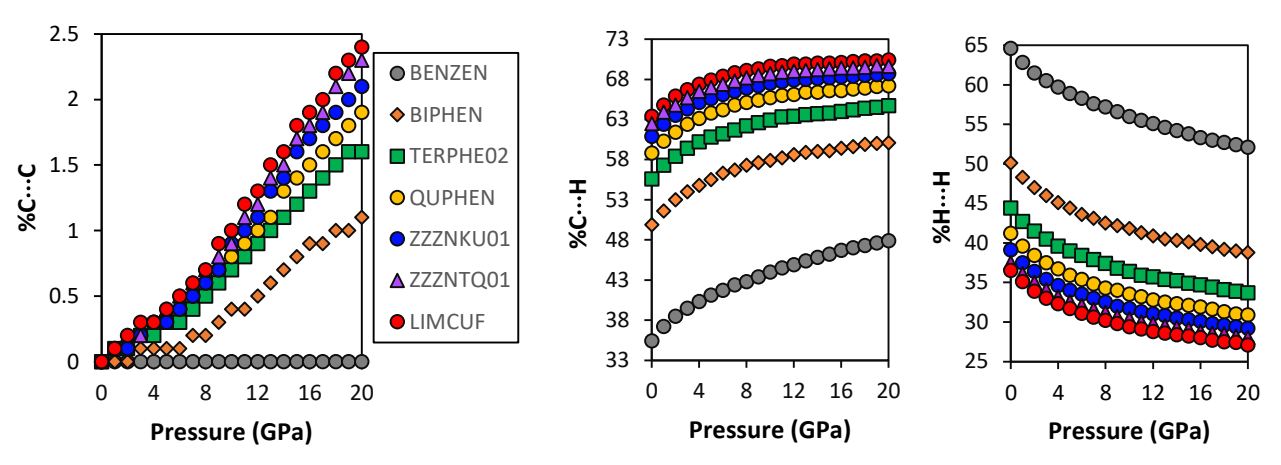


Figure 15. Intermolecular close contact fractions as a function of pressure for the poly(para-phenylenes).

It is important to note that the long molecular axes differ between the P_{21}/a and P_{21}/c space groups. For P_{21}/a , the long axis is aligned along c whereas in P_{21}/c it is aligned along a. This makes the second short molecular axis in P_{21}/a structures, a, and in P_{21}/c structures, c. Secondary axes are introduced into **Fig 14** to clarify the pressure dependent trends. From **Fig 14** it is evident that the unit cell axes associated with the second short axis (a or c) contract twice as much as a0 upon compression for all structures. This occurs because the molecules rotate around their long axis (aligned along a0 or a0, causing a tighter packing of the molecules within the unit cell. In the monoclinic structures, the short molecular axis (aligned along a0 has approximately the same length in each structure.

Based on the pressure dependence of the intermolecular close contact fractions shown in **Fig** 15, the poly(*para*-phenylenes) have slightly different pressure responses as the number of rings increases. The growth in %C···C surges with increasing number of rings, while the opposite is true for the %C···H. This occurs simply because the C/H ratio is increasing with increasing number of rings. Conversely, the pressure dependent decrease in the %H···H is nearly identical for all poly(*para*-phenylenes). This indicates that the entire poly(*para*-phenylene) family rotates about their long molecular axis to the same extent as seen in previous experimental work. 63

For all poly(para-phenylenes) the monoclinic angle, β , changes with increasing pressure, as seen in **Fig 16**. β , decreases by ~5° in 2P and ~6.5° in P6P as a function of pressure, while it increases in P3P, P4P, P5P, and P7P by ~4.5°. These changes have also been observed in experiment, where the increase/decrease of β was about 4°. The pressure dependent changes in β can be explained by the interlayer stacking of the molecules within the unit cell and their response to increaseing pressure. Representative structures of P2P and P7P at zero and 20 GPa are shown in **SI Fig S4**. When the pressure increases, molecules in P2P and P6P slide along the α direction which decreases β , whereas in P3P, P4P, P5P, and P7P molecules slide along the α direction, which increases β . Our findings regarding the change of β agree well with previous work.

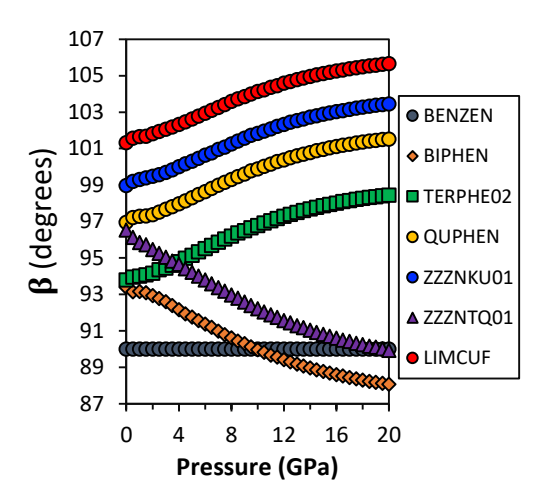


Figure 16. Lattice parameter β as a function of pressure for poly(*para*-phenylenes).

3.1.5 Phenacenes and asymmetric phenacenes: These HB-structures, shown in **Fig 17**, are characterized by benzene rings attached in a zigzag pattern. Phenacenes include phenanthrene (PHENAN), chrysene (CRYSEN01), and picene (ZZZOYC01). Asymmetric phenacenes include 1:2-benzanthracene (BEANTR) and dibenz[a,h]anthracene (DBNTHR02). All phenacenes crystallize in monoclinic structures: PHENAN and ZZZOYC01 have Z=2 and a P2₁ space group. While CRYSEN01 arranges into a C2/c space group with Z=4. The asymmetric phenacenes crystallize in various symmetry groups: BEANTR assembles into a monoclinic P2₁ space group with Z=2 and DBNTHR02 crystallizes into an orthorhombic P*bca* space group with Z=4.

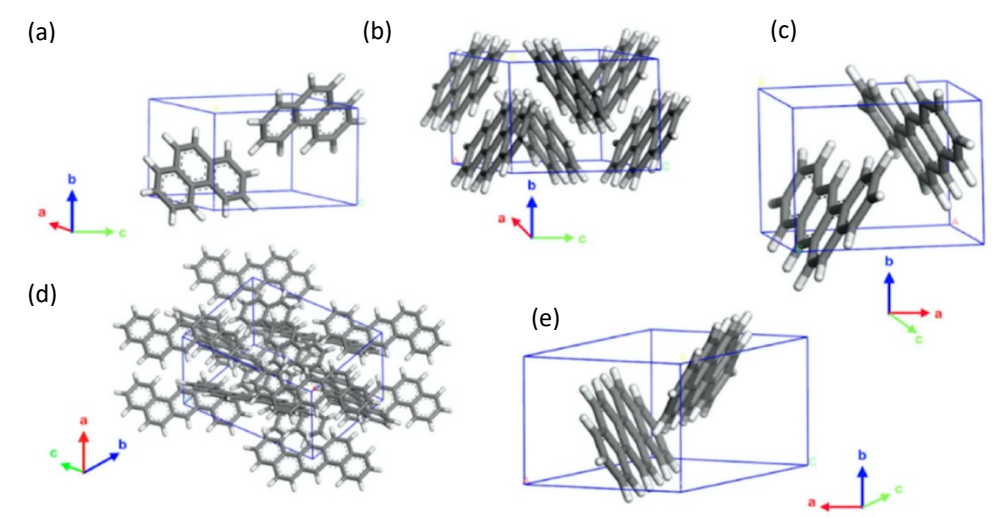


Figure 17. Crystal structure of (a) PHENAN, (b) CRYSEN01, (c) BEANTR, (d) DBNTHR02, and (e) ZZZOYC01 at ambient pressure.

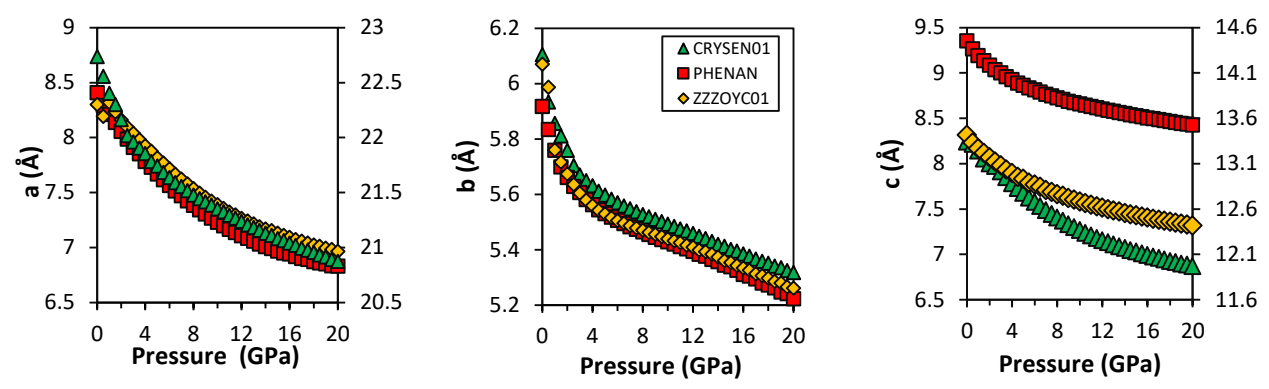


Figure 18. Lattice parameters as a function of pressure for phenanthrene (PHENAN), chrysene (CRYSEN01), and picene (ZZZOYC01). CRYSEN01 is on the secondary axis for *a*. ZZZOYC01 is on the secondary axis for *c*. Secondary and primary axis are on the same scale.

The unit cell parameters a, b, and c as a function of pressure for the phenancenes are plotted in Fig 18. For the phenancenes, a, b, and c follow a predictable exponential decay, where all structures undergo approximately the same magnitude of change in a and b with a slight variation in c for CRYSEN01. Comparison of the calculated and experimental unit cell volume of phenacene is shown in SI Fig S3. Excellent agreement is obtained up to about 14 GPa, at which point a phase transition is observed experimentally. This discrepancy may be the result of the DFT calculations being conducted at 0K, as explained above. Still, even above 14 GPa, the calculated and experimental volumes differ by less than 5%. Small discontinuities in a and b for ZZZOYC01 from 0.5-1.0 GPa hint at a phase transition, though no change in space group is observed. This compares well with experimentally observed changes in the two-photon-excitation profiles which occur between 0.1 and 1.5 GPa. The phase transition is characterized by molecular slips along b and c, as well as an increase of the interplanar angle (towards 90 degrees) which elongates a. Representative figures of the phase transitions can be seen in SI Fig 13.

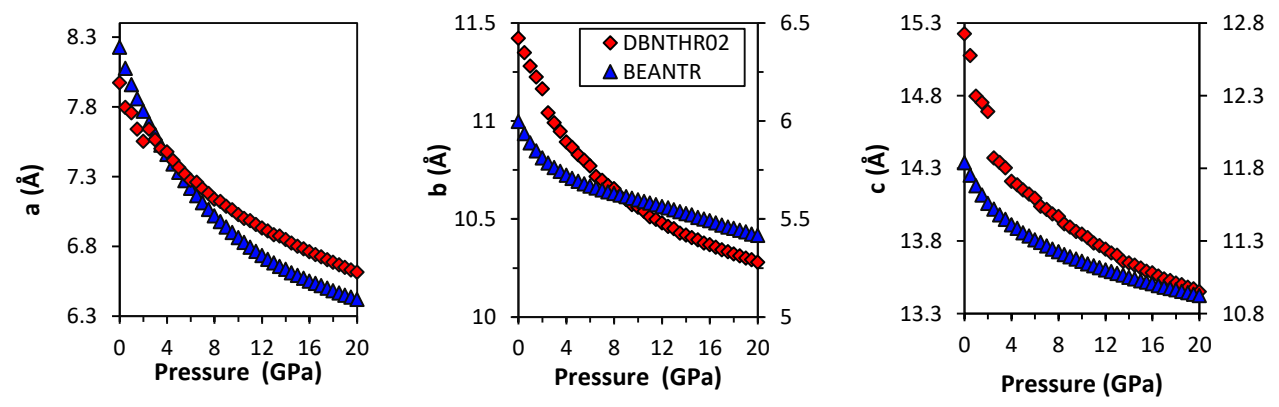


Figure 19. Lattice parameters as a function of pressure for BEANTR and DBNTHR02. BEANTR on the secondary axis for **b** and **c**. Primary and secondary axes on the same scale.

The pressure dependence of the unit cell parameters a, b, and c for the asymmetric phenacenes is plotted in **Figs 19**. The magnitude change for all parameters is comparable to the symmetric phanacenes. It is interesting to note that there are discontinuities in the pressure dependence of the lattice parameters of DBNTHR02 between 2-2.5 GPa, suggesting that a phase transition may occur (no change in space group observed). The phase transition of DBNTHR02

is similar in nature to that of ZZZOYC01 above and is characterized by a molecular slip along b, accompanied with an increase of the interplanar angle (towards 90 degrees) which elongates a. Representative figures of the phase transitions can be seen in SI Fig 14.

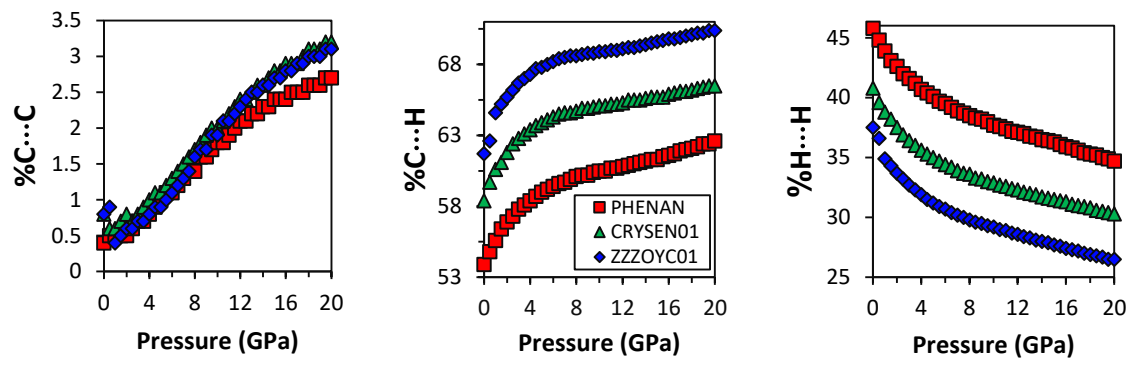


Figure 20. Relative intermolecular close contact fractions as a function of pressure for the phenanthrenes.

The pressure dependence of the intermolecular close contact fractions for the phenacenes is presented in **Fig 20**. Here, the general trends of increasing %C···C and %C···H, accompanied by decreasing %H···H, is observed with one notable exception. For ZZZOYC01, a discontinuity in the curves is found between 0.5 and 1.0 GPa. This discontinuity correlates with the phase transition, where the increase in the interplanar angle decreases face-to-face interactions, leading to a discontinuous decrease in C···C contacts and discontinuous increases in C···H and H···H contacts. Beyond 1 GPa, the pressure dependence of the close contacts of all three phenacenes is nearly identical with respect to the percent change and the shape of the curve. The variation in the %C···H and %H···H starting values is simply a result of the increasing C/H ratio as more rings are added.

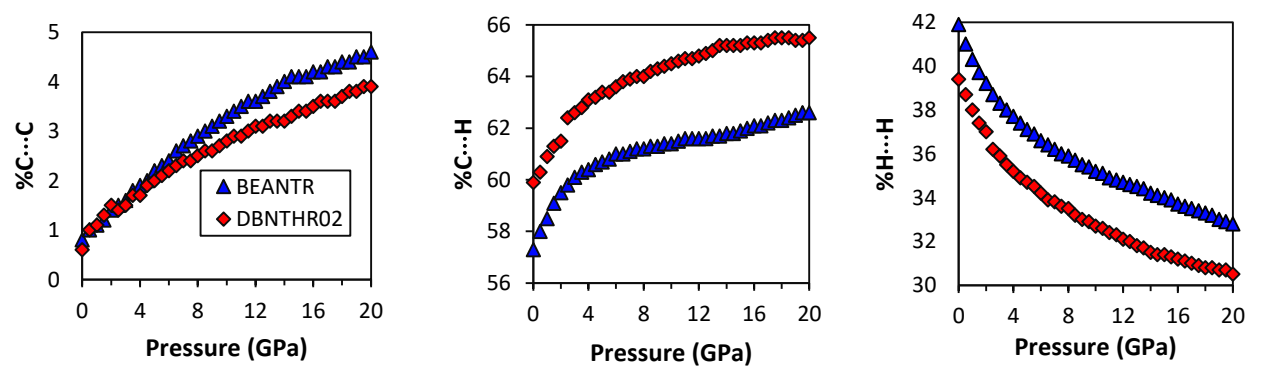


Figure 21. Relative intermolecular close contact fractions as a function of pressure for BEANTR and DBNTHR02.

The pressure dependence of the intermolecular close contact fractions for the asymmetric phenacenes is presented in **Fig 21**. Here the general trend of increasing %C···C and %C···H, with decreasing %H···H is observed, with the exception of the discontinuities for all contacts of DBNTHR02 from 2 to 2.5 GPa. These discontinuities correlate with the phase transition, where the increase in the interplanar angle decreases face-to-face interactions, leading to a discontinuous decreases in C···C and H···H contacts and a discontinuous increase in C···H

contacts. It is interesting to note that the phase transitions in the phenacenes, asymmetric phenacenes, triphenylenes, and phenyl substituted acenes only emerge for structures with at least five rings in the acene structures.

3.1.6. 1,8-Dipyrenylnaphthalenes: This family of HB-PAHs is a series of stereo and structural isomers characterized by forced π - π interactions between pyrene units bound to a naphthalene backbone, as seen in **Fig 22**. It has been shown experimentally that the optical properties of these isomers are quite different, owing to variations in excimer interactions between the pyrene moieties. ⁶⁶ CENXUO and CENYAV are considered stereo isomers while CENYEZ is a structural isomer. The structures assemble into monoclinic arrays with two and four molecules per unit cell [CENYEZ = P2₁/n (Z=4), CENYAV = P2₁ (Z = 2), and CENXUO = P2₁/c (Z=4)].

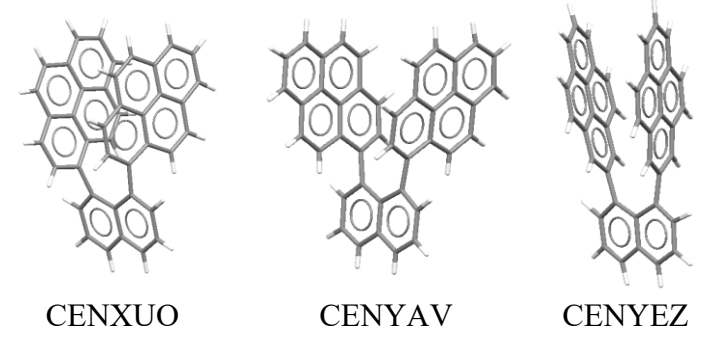


Figure 22. Molecular structures of the 1,8-dipyrenylnaphthalenes, CENXUO, CENYAV, and CENYEZ as extracted from the crystal structure at 0 GPa.

The pressure dependent plots of a, b, and c for the 1,8-dipyrenylnaphthalenes are shown in Fig 23. The stereo isomers, CENXUO and CENYAV, exhibit significantly different pressure responses, but both structures exhibit phase transition behavior at similar pressures, though no space group transformation is observed. CENXUO shows a nearly continuous decrease in a, b, and c, but small discontinuities between 10.5 to 11 GPa are observed for all parameters, hinting at a phase transition. The phase transition is characterized by a slip of the molecules in the a-c plane. Conversely, CENYAV exhibits large discontinuities in all lattice parameters between 9.5 to 10 GPa (despite the absence of space group change), strongly suggesting a phase transition. The phase transition is characterized by molecular rotations, slips, and deformations. rotation is characterized by the angle between the naphthalene moieties increasing (going towards 90 degrees). The slip is characterized by the entire molecule slipping in planes, increasing β by nearly 1 degree. The molecular deformations are characterized by the pyrene moieties i) twisting and ii) being forced more to one side of the naphthalene component. The pressure dependence of the lattice parameters of the structural isomer, CENYEZ, is most similar to CENXUO in both magnitude and shape. A small discontinuous change in c between 8.5 to 9.0 GPa hints at a phase transition for CENYEZ, and leads to large changes in the intermolecular close contact fractions in this same pressure range (no change in space group observed). The phase transition is characterized by a slip of the molecules in the a-c plane which increases β , though no change in space group is observed. Representative figures of the phase transitions for CENYAV and CENXUO can be found in SI Figs S15 - S17.

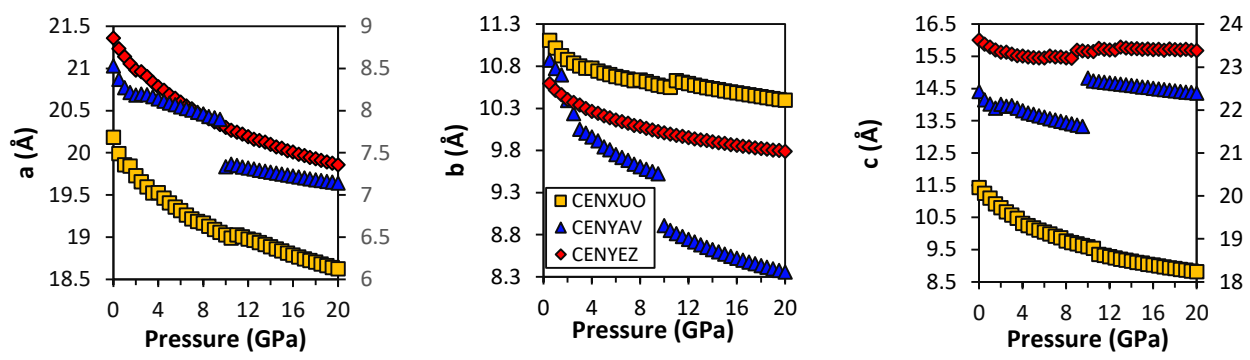


Figure 23. Lattice parameters as a function of pressure for the 1,8-dipyrenylnaphthalenes, CENYAV, CENYEZ, and CENXUO. CENYAV is plotted on the secondary axis for a. CENYEZ is plotted on the secondary axis for c. Primary and secondary axes on the same scale.

Fig 24 presents the pressure dependence of the intermolecular close contact fractions for the 1,8-dipyrenylnaphthalenes. Here the general trends of increasing %C···C and %C···H, with decreasing %H···H, is observed with some notable variations. CENXUO shows continuous changes in the intermolecular close contact fractions, with negligible discontinuities in %C···C and %C···H between 10.5 to 11 GPa associated with the phase transition. The stereo isomer, CENYAV, exhibits typical close contact variation up to a series of large discontinuities in all fractions between 9.5 and 10 GPa, indicative of the phase transition. The structural isomer, CENYEZ, shows typical close contact behavior up to the discontinuities between 8.5 and 9 GPa. Above 9 GPa, the %C···C and %H···H continue to follow the typical trend. However, the %C···H undergoes an atypical decrease above 9 GPa.

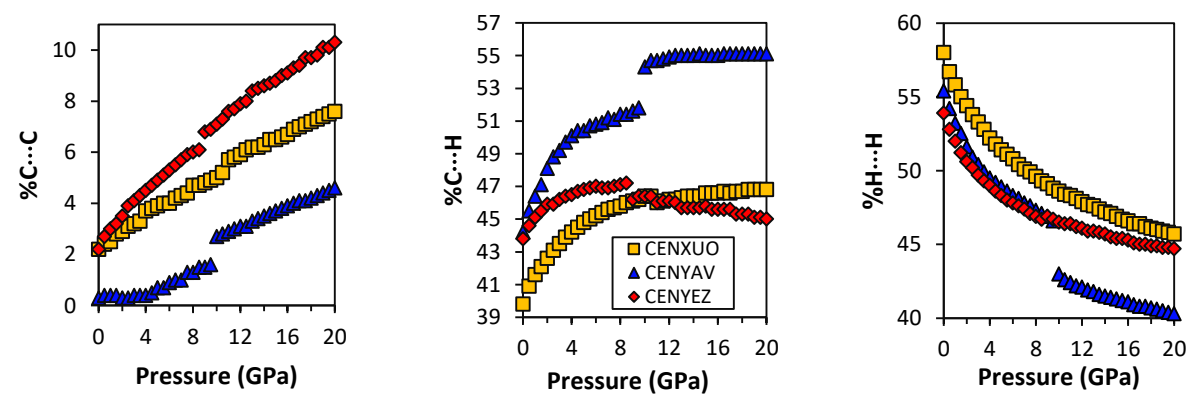


Figure 24. Relative intermolecular close contact fractions as a function of pressure for CENYAV, CENYEZ, and CENXUO

3.1.7. Oligoacenes: We have investigated the structural and electronic responses of this family up to 25 GPa previously;¹⁹ where very good agreement was observed between experiment and our calculations. In Figures 1-3 of Ref. 41, the structural change as a function of pressure are plotted for naphthalene (2A), anthracene (3A), tetracene (4A), and pentacene (5A). Agreement between the experiment and calculated values of the structural parameters is within ~2%. Furthermore, as a result of applying pressure, the fraction of H···H interactions decreases for all structures while the C···H and C···C interactions increase. It was observed that tetracene

undergoes a phase transition above 6 GPa as shown in experiment.⁶⁷ Animation of the tetracene phase transition can be found in the **ESI**.

4. Conclusion

We have investigated the structural pressure response of 42 different herringbone PAH crystals, using dispersion-corrected DFT. Several characteristic trends have been identified in the change of the lattice parameters and the intermolecular close contact interactions with increased pressure. The lattice parameters typically decrease exponentially with the axis associated with the π -stacking direction decreasing about twice as much as the other unit cell axes. The interplanar angle of the molecules in the stack decreases, increasing the coplanarity of the molecules and the packing efficiency. This manifests as an increase in C···C and C···H intermolecular close contact fractions and a decrease in H···H interactions which helps alleviate electrostatic repulsions. While the behavior of most structures was consistent with these trends, some were found to exhibit discontinuities in the lattice parameters and the corresponding Hirshfeld intermolecular close contact fractions. Such discontinuities in the structural descriptors are typically indicative of phase transitions, however it is important to note that despite our previous success capturing phase transition behavior via electronic structure calculations, DFT performed at 0 K does not capture the free energy contribution. We have further conducted detailed analyses of trends across well known HB-PAH families. It is interesting to note that aside from the oligoacenes, no structures from any family underwent pressure induced phase transitions that had less than five rings. In the second part of this study we analyze the response the electronic properties of these crystals under pressure.

Acknowledgements

Work at CPP by BS was funded by National Science Foundation (NSF) Division of Materials Research through grant DMR-1637026. NM acknowledges support from the NSF Division of Materials Research through grant DMR-1554428.

Supporting Information Available: [...]

References

- Schatschneider, B.; Phelps, J.; Jezowski, S. A New Parameter for Classification of Polycyclic Aromatic Hydrocarbon Crystalline Motifs: a Hirshfeld Surface Investigation. *CrystEngComm.* **2011**, 13, 7216-7223.
- Desiraju, G. R.; Gavezzotti, A. From Molecular to Crystal Structure; Polynuclear Aromatic Hydrocarbons. *J. Chem. Soc. Chem. Commun.* **1989**, 0, 621-623.
- Desiraju, G. R.; Gavezzotti, A.; Crystal Structures of Polynuclear Aromatic Hydrocarbons. Classification, Rationalization and Prediction from Molecular Structure. *Acta Crystallogr. Sect. B Struct. Sci.* **1989**, 45, 473–482.
- 4 Desiraju, G.R. Crystal engineering: the design of organic solids; Elsevier, 1989.
- Fabbiani, F. P. A.; Allan, D. R.; Parsons, S.; Pulham, C. R. Exploration of the High-Pressure Behaviour of Polycyclic Aromatic Hydrocarbons: Naphthalene, Phenanthrene and Pyrene. *Acta Crystallogr. Sect. B Struct. Sci.* **2006**, B62, 826–842.
- 6 Schatschneider, B.; Monaco, S.; Liang, J.-J.; Tkatchenko, A. High-Throughput Investigation of the Geometry and Electronic Structures of Gas-Phase and Crystalline Polycyclic Aromatic Hydrocarbons. *J. Phys. Chem. C* **2014**, 118 (34), 19964–19974.
- Prédas, J. L.; Calbert, J. P.; da Silva Filho, D. A.; Cornil, J. Organic Semiconductors: A Theoretical Characterization of the Basic Parameters Governing Charge Transport. *Proc. Natl. Acad. Sci. U. S. A.* **2002**, 99, 5804–5809.
- Wang, X. F.; Liu, R. H.; Gui, Z.; Xie, Y. L.; Yan, Y. J.; Ying, J. J.; Luo, X. G.; Chen, X. H. Superconductivity at 5 K in Alkali-Metal-Doped Phenanthrene. *Nat. Commun.* **2011**, 2, 507.
- 9 Liu, T.; Xu, S.; Sun, C.; Zhou, M. Gas Sensing in 2d Materials. *Chem. Phys. Lett.*, **2014**, 615, 1–5.
- Schatschneider, B; Chronister, E. L. Molecular Simulation of the Pressure-Induced Crystallographic Phase Transition of p-terphenyl. *J. Phys. Chem. B* **2011**, 115, 407–413.
- Zhao, X. M.; Zhang, J.; Berlie, A.; Qin, Z. X.; Huang, Q. W.; Jiang, S.; Zhang, J. B.; Tang, L. Y.; Liu, J.; Zhang, C.; Zhong, G. H.; Lin, H. Q.; Chen, X. J. Phase Transformations and Vibrational Properties of Coronene Under Pressure. *J. Chem. Phys.* **2013**, 139, 144308.
- Heimel, G.; Puschnig, P.; Oehzelt, M.; Hummer, K.; Koppelhuber-Bitschnau, B.; Porsch, F.; Ambrosch-Draxl, C.; Resel, R. Chain-Length-Dependent Intermolecular Packing in Polyphenylenes: a High Pressure Study. *J. Phys. Condens. Matter.* **2003**, 15 (20), 3375–3389.
- Oehzelt, M.; Aichholzer, A.; Resel, R.; Heimel, G.; Venuti, E.; Della Valle, R. G. Crystal Structure of Oligoacenes Under High Pressure. *Phys. Rev. B* **2006**, 74, 104103.
- Bergantin, S.; Moret, M.; Buth, G.; Fabbiani, F. P. A. Pressure-Induced Conformational Change in Organic Semiconductors: Triggering a Reversible Phase Transition in Rubrene. *J. Phys. Chem. C* **2014**, 118 (25), 13476–13483.
- Schatschneider, B.; Liang, J. J. Simulated Pressure Response of Crystalline Indole. *J. Chem. Phys.* **2011**, 135, 164508.
- Fanetti, S.; Citroni, M.; Malavasi, L.; Artioli, G. A.; Postorino, P.; Bini, R. High-Pressure Optical Properties and Chemical Stability of Picene. *J. Phys. Chem. C*, **2013**, 117 (10), 5343–5351.
- 17 Capitani, F.; Höppner, M.; Malayasi, L.; Marini, C.; Artioli, G. A.; Hanfland, M.; Dore,

- P.; Boeri, L.; Postorino, P. Structural Evolution of Solid Phenanthrene at High Pressures. *J. Phys. Chem. C* **2016**, 120 (26), 14310–14316.
- 18 Radisavljevic, I.; Marjanovic, D.; Novakovic, N.; Ivanovic, N. Changes in Structure and Properties of Oligophenylenes under Selected External Influences. *Mater. Sci. Forum.* **2007**, 555, 509–514.
- Schatschneider, B.; Monaco, S.; Tkatchenko, A.; Liang, J.-J. Understanding the Structure and Electronic Properties of Molecular Crystals Under Pressure: Application of Dispersion Corrected DFT to Oligoacenes. *J. Phys. Chem. A*, **2013**, 117 (34), 8323–8331.
- 20 Xiao, L.-P.; Zhong, G.-H.; Zeng, Z.; Chen, X.-J. Theoretical Study on Structural and Electronic Properties of Solid Anthracene Under High Pressure by Density Functional Theory. *Mol. Phys.* **2016**, 114, 283–289.
- Zhao, X.-M.; Zhong, G.-H.; Zhang, J.; Huang, Q.-W.; Goncharov, A. F.; Lin, H.-Q.; Chen, X.-J. Combined Experimental and Computational Study of High-Pressure Behavior of Triphenylene. *Sci. Rep.*, **2016**, 6, 25600.
- Wang, X.; Garcia, T.; Monaco, S.; Schatschneider, B.; Marom, N. Effect of Crystal Packing on the Excitonic Properties of Rubrene Polymorphs. *CrystEngComm*, **2016**, 18, 7353–7362.
- Casati, N.; Kleppe, A.; Jephcoat, AP.; Macchi, P. Putting pressure on aromaticity along with in situ experimental electron density of a molecular crystal. *Nat. Commun.* **2016**, 7, 10901.
- Cai, W.; Zhang, R.; Yao, Y. Piezochromism and Structural and Electronic Properties of Benz[a]anthracene Under Pressure. *Phys. Chem. Chem. Phys.* **2017**, 19, 6216–6223.
- Mitsuhashi, R.; Suzuki, Y.; Yamanari, Y.; Mitamura, H.; Kambe, T.; Ikeda, N.; Okamoto, H.; Fujiwara, A.; Yamaji, M.; Kawasaki, N.; Maniwa, Y.; Kubozono, Y. Superconductivity in Alkali-Metal-Doped Picene. *Nature*, **2010**, 464, 76–79.
- Oehzelt, M.; Heimel, G.; Resel, R.; Puschnig, P.; Hummer, K.; Ambrosch-Draxl, C.; Takemura, K.; Nakayama, A. High Pressure X-ray Study on Anthracene. *J. Chem. Phys.* **2003**, 119, 1078–1084.
- B. Schatschneider, J.-J. Liang, S. Jezowski, A. Tkatchenko. Phase Transition Between Cubic and Monoclinic Polymorphs of the Tetracyanoethylene Crystal: the Role of Temperature and Kinetics. *CrystEngComm.* **2012**, 14, 4656-4663.
- Perdew, J.; Bruke, K.; Ernzerhof, M. Generalized Gradient Approximation Made Simple. *Phys. Rev. Lett.* **1996**, 77, 3865–3868.
- Tkatchenko, A.; Scheffler, M. Accurate Molecular Van Der Waals Interactions from Ground-State Electron Density and Free-Atom Reference Data. *Phys. Rev. Lett.* **2009**, 102, 073005.
- Allen, F. H. The Cambridge Structural Database: a quarter of a million crystal structures and rising. *Acta Crystallogr. Sect. B Struct. Sci.* **2002**, 58, 380–388.
- Oehzelt, M.; Aichholzer, A.; Resel, R.; Heimel, G.; Venuti, E; Della Valle, R. G. Crystal Structure of Oligoacenes Under High Pressure. *Phys. Rev. B* **2006**, 74, 104103.
- Huang, L.; Liao, Q.; Shi, Q.; Fu, H.; Ma, J.; Yao, J. Rubrene Micro-Crystals from Solution Routes: Their Crystallography, Morphology and Optical Properties. *J. Mater. Chem.* **2010**, 20, 159–166.
- Clark, S. J.; Segall, M. D.; Pickard, C. J.; Hasnip, P. J.; Probert, M. J.; Refson, K.; Payne M. C. First principles methods using CASTEP. Zeitschrift fuer Kristallographie. **2005**, 220, 567-570.

- Monkhorst, H. J.; Pack, J. D. Special Points for Brillouin-Zone Integrations *Phys. Rev. B* **1976**, 13, 5188–5192.
- Pfrommer, B. G.; Côté, M.; Louie, S. G.; Cohen, M. L. Relaxation of Crystals with the Quasi-Newton Method. *J. Comput. Phys.* **1997**, 131, 233–240.
- Groom, C. R.; Bruno, I. J.; Lightfoot, M. P.; Ward, S. C. The Cambridge Structural Database. *Acta Crystallogr B Struct Sci Cryst Eng Mater.* **2016**, 72, 171-179
- Wolff, S.K.; Grimwood, D.J.; McKinnon, J.J.; Turner, M.J.; Jayatilaka, D.; Spackman, M.A. CrystalExplorer (Version 3.1). University of Western Australia. **2012**.
- Spackman, M. A.; Jayatilaka, D. General Paper on Hirshfeld Surface Analysis. *CrystEngComm*, 2009, **11**, 19-32.
- Wood, P. A.; McKinnon, J. J.; Parsons, S.; Pidcock, E.; Spackman, M. A. Analysis of the Compression of Molecular Crystal Structures Using Hirshfeld Surfaces. *CrystEngComm* **2008**, 10, 368–376.
- McKinnon, J.J.; Jayatilaka, D.; Spackman, M. A. d_{norm} and Fingerprint Breakdown *Chem. Commun.* **2007**, 3814–3816.
- 41 Schatschneider, B.; Monaco, S.; Tkatchenko, A.; Liang, J.- J. Understanding the Structure and Electronic Properties of Molecular Crystals Under Pressure: Application of Dispersion Corrected DFT to Oligoacenes. *J. Phys. Chem. A* **2013**, 117 (34), 8323–8331.
- Sun, Z.; Wang, J.; Ye, S.; Jiang, C.; Chen, H. Effects of Hydrostatic Pressure on the Excitation-Emission Matrix (EEM) of a Series of Pure PAHs. *J. Lumin.* **2017**, 186, 77–86.
- Abdulla, M.; Refson, K.; Friend, R. H.; Haynes, P. D. A first-principles study of the vibrational properties of crystalline tetracene under pressure. *J. Phys.: Condens. Matter* **2015**, 27, 375402.
- Capitani, F.; Höppner, M.; Joseph, B.; Malavasi, L.; Artioli, G. A.; Baldassarre, L.; Perucchi, A.; Piccinini, M.; Lupi, S.; Dore, P.; Boeri, L.; Postorino, P. A Combined Experimental and Computational Study of the Pressure Dependence of the Vibrational Spectrum of Solid Picene C₂₂H₁₄. *Phys. Rev. B* **2013**, 88, 144303.
- Ward, K. A.; Richman, B. R.; Biaggio, I. Nanosecond Pump and Probe Observation of Bimolecular Exciton Effects in Rubrene Single Crystals. *Appl. Phys. Lett.* **2015**, 106, 223302.
- Biaggio I.; Irkhin, P. Extremely Efficient Exciton Fission and Fusion and its Dominant Contribution to the Photoluminescence Yield in Rubrene Single Crystals. *Appl. Phys. Lett.* **2013**, 103, 263301.
- 47 Ryasnyanskiy, A.; Biaggio, I. Triplet exciton dynamics in rubrene single crystals. *Phys. Rev. B* **2011**, 84, 193203.
- 48 Ma, L.; Zhang, K.; Kloc, C.; Sun, H.; Soci, C.; Michel-Beyerle, M. E.; Gurzadyan, G. G. Fluorescence from Rubrene Single Crystals: Interplay of Singlet Fission and Energy Trapping. *Phys. Rev. B* **2013**, 87, 201203.
- Collings, J. C.; Roscoe, K. P.; Thomas, R. L.; Batsanov, A. S.; Stimson, L. M.; Howard, J. A. K.; Marder, T. B. Arene-perfluoroarene Interactions in Crystal Engineering. Part 3. Single-crystal Structures of 1:1 Complexes of Octafluoronaphthalene with Fused-ring Polyaromatic Hydrocarbons. *New J. Chem.* **2001**, 25, 1410–1417.
- 50 Salzillo, T.; Della Valle, R. G.; Venuti, E.; Brillante, A.; Siegrist, T.; Masino, M.; Mezzadri, F.; Girlando, A. Two New Polymorphs of the Organic Semiconductor 9,10-Diphenylanthracene: Raman and X-ray Analysis. *J. Phys. Chem. C* **2016**, 120 (3), 1831–1840.

- Jurchescu, O. D.; Meetsma, A.; Palstra, T. T. M. Low-temperature Structure of Rubrene Single Crystals Grown by Vapor Transport. *Acta Crystallogr. Sect. B Struct. Sci.* **2006**, 62, 330–334.
- Miao, Q.; Chi, X.; Xiao, S.; Zeis, R.; Lefenfeld, M.; Siegrist, T.; Steigerwald, M. L.; Nuckolls, C. Organization of Acenes with a Cruciform Assembly Motif. *J. Am. Chem. Soc.* **2006**, 128 (4), 1340-1345.
- Fernandes, P.; Florence, A.; Shankland, K.; David, W. I. F. Powder diffraction study of 1,2:3,4- dibenzanthracene. *Acta Crystallogr. Sect. E* **2005**, 61, o1483–o1485.
- Saleh, M.; Baumgarten, M.; Mavrinskiy, A.; Schäfer, T.; Müllen, K. Triphenylene-Based Polymers for Blue Polymeric Light Emitting Diodes. *Macromolecules* **2010**, 43 (1), 137–143.
- Shih, H. T.; Shih, H.-H.; Cheng, C.-H. Synthesis of Biaryls via Unusual Deoxygenative Dimerization of 1,4-Epoxy-1,4-dihydroarenes Catalyzed by Palladium Complexes. *Org. Lett.* **2001**, 3 (6), 811-814.
- Shih, H.-T.; Lin, C.-H.; Shih, H.-H.; Cheng, C.-H. High-Performance Blue Electroluminescent Devices Based on a Biaryl. *Adv. Mater.* **2002**, 14 (19), 1409–1412.
- 57 McKenna, M. D.; Barberá, J.; Marcos, M.; Serrano, J. L. Discotic Liquid Crystalline Poly(propylene imine) Dendrimers Based on Triphenylene. *J. Am. Chem. Soc.* **2005**, 127 (2), 619-625.
- Trotter, J. The Crystal and Molecular Structure of Biphenyl. *Acta Crystallogr.* **1961**, 14, 1135–1140.
- Rietveld, H. M.; Maslen, E. N.; Clews, C. J. B. An X-ray and neutron diffraction refinement of the structure of p-terphenyl. *Acta Crystallogr. Sect. B* **1970**, 26, 693–706.
- Delugeard, Y.; Desuche, J.; Baudour, J. L. Structural Transition in Polyphenyls. II. The Crystal Structure of the High-Temperature Phase of Quaterphenyl. *Acta Crystallogr. Sect. B* **1976**, 32, 702–705.
- Baker, K. N.; Fratini, A. V.; Resch, T.; Knachel, H. C.; Adams, W. W.; Socci, E. P.; Farmer, B. L. Crystal Structures, Phase Transitions and Energy Calculations of Poly(p-phenylene) Oligomers. *Polymer* **1993**, 34 (8), 1571–1587.
- Bacon, G. E.; Curry, N. A.; Wilson, S. A. A Crystallographic Study of Solid Benzene by Neutron Diffraction. *Proc. R. Soc. Lond. A* **1964**, 279, 1376.
- Zhou, M.; Wang, K.; Men, Z.; Gao, S.; Li, Z.; Sun, C. Study of High-Pressure Raman Intensity Behavior of Aromatic Hydrocarbons: Benzene, Biphenyl and Naphthalene. *Spectrochim. Acta Part A: Mol. Biomol. Spectrosc.* **2012**, 97, 526–531.
- Trotter, J. Bond Lengths and Angles in Pentaerythritol Tetranitrate. *Acta Cryst.* **1963**, 16, 698-699.
- De, A.; Ghosh, R.; Roychowdhury, S.; Roychowdhury, P. Structural Analysis of Picene, C₂₂H₁₄. *Acta Crystallogr. Sect. C* **1985**, 41, 907–909.
- Wahl, P.; Krieger, C.; Schweitzer, D.; Staab, H. A. 1,8-Dipyrenylnaphthalenes: Syntheses, Molecular Structure, and Spectroscopic Properties. *Chem. Ber.* **1984**, 117, 1, 260–276.
- Venuti, E.; Della Valle, R. G.; Farina, L.; Brillante, A.; Masino, M.; Girlando, A. Phonons and structures of tetracene polymorphs at low temperature and high pressure. *Phys. Rev. B* **2004**, 70, 104106.